Atmos. Chem. Phys. Discuss., 13, 31563–31605, 2013
www.atmos-chem-phys-discuss.net/13/31563/2013/
doi:10.5194/acpd-13-31563-2013

Atmospheric Chemistry and Physics Discussions

Ozone vegetation damage effects on gross primary productivity in the United States

X. Yue and N. Unger

School of Forestry and Environmental Studies, Yale University, 195 Prospect Street, New Haven, CT 06511, USA

Received: 14 November 2013 – Accepted: 18 November 2013 – Published: 2 December 2013

Correspondence to: X. Yue (xu.yue@yale.edu)

Published by Copernicus Publications on behalf of the European Geosciences Union.

Abstract

We apply an off-line process-based vegetation model to assess the impacts of ozone (O_3) vegetation damage on gross primary productivity (GPP) in the United States (US) during the past decade (1998–2007). The model's GPP simulation is evaluated at 40 sites of the North American Carbon Program (NACP) synthesis. The ecosystem-scale model version reproduces interannual variability and seasonality of GPP at most sites, especially in croplands. Inclusion of the O_3 damage impact decreases biases of simulated GPP at most of the NACP sites. The simulation with the O_3 damage effect reproduces 64 % of the observed variance in summer GPP and 45 % on the annual average. Based on a regional gridded simulation over the US, summertime average O_3-free GPP is 5.9 g C m^{-2} day^{-1} (9.1 g C m^{-2} day^{-1} in the East of 95° W and 3.7 g C m^{-2} day^{-1} in the West). O_3 damage decreases GPP by 3–7 % on average in the eastern US and leads to significant decreases of 13–17 % in east coast hotspots. Sensitivity simulations show that a reduction of 25 % in surface O_3 concentration alleviates the average GPP damages to 1–3 %, suggesting a promising prospect for ecosystem health following the emission control.

1 Introduction

The effects of tropospheric ozone (O_3) damage on US forests have been studied for half a century (Karnosky et al., 2007), but the impacts of O_3 on the North American carbon balance are still relatively poorly understood (Felzer et al., 2004; Sitch et al., 2007; Huntingford et al., 2011). O_3 is a secondary pollutant produced in the troposphere during the photochemical oxidation of carbon monoxide, methane, and volatile organic compounds (VOCs) by the major tropospheric oxidant, the hydroxyl radical, in the presence of sunlight and nitrogen oxides. Fossil-fuel, biofuel and biomass burning since the industrial and agricultural revolutions have greatly increased the emissions of O_3 precursors and led to an approximate doubling of O_3 levels over the US since

ACPD
13, 31563–31605, 2013

the preindustrial. Deposition through stomatal uptake is an important sink for O_3 but damages photosynthesis, reduces plant growth and biomass accumulation, limits crop yields, and affects stomatal control over plant transpiration of water vapor between the leaf surface and atmosphere (Ainsworth et al., 2012; Hollaway et al., 2012).

Understanding the O_3 pollution influence on the North American forest sink is crucial to any effort to mitigate climate change by stabilizing atmospheric carbon dioxide (CO_2) concentrations. Sequestration of atmospheric CO_2 by forest ecosystems is a major control on atmospheric CO_2 abundance and its growth rate (Pan et al., 2011). US regional climate change over the 21st century depends on the rate at which anthropogenic CO_2 emissions are removed from the atmosphere by the land carbon cycle. Currently, North America is acting as a net source of CO_2 to the atmosphere (King et al., 2012). Terrestrial ecosystems of North America absorb the equivalent of about 35 % of North America's fossil fuel based CO_2 emissions, representing a source-to-sink ratio of nearly 3 : 1. Forest regrowth in the US is responsible for 30–70 % of this North American CO_2 sink, which varies significantly from year to year (Pacala et al., 2001; Goodale et al., 2002; Pan et al., 2011; King et al., 2012). Worse still, there is evidence that the summer continental US is more sensitive than other world regions to climate forcing (Levy et al., 2008).

Experimental studies that examine O_3 impacts on plant productivity are typically performed for individual vegetation types, on the scale of sites, and within a limited time period (e.g. Wittig et al., 2007; Feng et al., 2008; Lombardozzi et al., 2013). For example, based on measurements reported from over 100 studies, Wittig et al. (2007) estimated that chronic O_3 exposure depressed photosynthesis by 11 % and stomatal conductance by 13 % for several tree species at the ambient O_3 level of ∼ 45 ppbv relative to that in O_3-free air. The O_3 damage effect is strongest for crops. With datasets from ∼ 50 peer-reviewed studies, Feng et al. (2008) estimated that elevated O_3 levels significantly decrease wheat photosynthetic rates by 20 % and stomatal conductance by 22 %.

ACPD
13, 31563–31605, 2013

Previous work has found that in the US region during 1989–1993, O_3 pollution reduced net primary productivity (NPP) by 3–7 % overall, and up to 13 % in hotspots including the southeast and in the Midwest agricultural lands (Felzer et al., 2004, 2005). The indirect CO_2 radiative forcing due to the vegetation damage effects of anthropogenic O_3 increases since the industrial revolution may be as large as +0.4 Wm^{-2} (Sitch et al., 2007), which is 25 % of the magnitude of the direct CO_2 radiative forcing over the same period, and of similar magnitude to the direct O_3 radiative forcing. Through this perturbation of the carbon cycle, O_3 pollution affects the climate system on considerably longer timescales than its own atmospheric lifetime (Unger and Pan, 2012).

Over the past decade since this previous assessment surface O_3 levels in most of the US have decreased (Lefohn et al., 2010) due to domestic emission reductions following the implementation of air quality control legislation (Bloomer et al., 2010). However, increasing O_3 concentration is observed over western US (Jaffe and Ray, 2007). Such a trend may in part be related to the inter-continental flow from Asia (Cooper et al., 2010) and the global increase in methane (Rigby et al., 2008).

The major goal of this study is to assess O_3 damage effects on gross primary productivity (GPP) in the US for the recent decade 1998–2007 using a data-constrained vegetation model. In this work, we describe the implementation of a semi-mechanistic O_3 damage function (Sitch et al., 2007) into a vegetation model that includes enzyme-kinetic biophysics (Unger et al., 2013). In the first stage of the study, we utilize eddy-derived GPP flux measurements at 40 sites across the US and Canada that have been collated for the North American Carbon Program (NACP) site-level interim synthesis (Huntzinger et al., 2012; Schaefer et al., 2012; Barr et al., 2013; Ricciuto et al., 2013) to evaluate an off-line version of the vegetation model's site level GPP simulation and to quantify the impact of surface O_3 damage at those sites. In the second stage of the study, the impacts of O_3 damage on GPP throughout the entire US region are quantified using a regionally distributed configuration of the vegetation model. In Sect. 2, we describe the vegetation model, the implementation of the O_3 damage scheme, the

ACPD
13, 31563–31605, 2013

meteorological forcing, and the specific configurations of the site-level and regionally distributed simulations. Results are presented in Sect. 3, including O_3-free and O_3-damaged GPP at NACP sites and for the US region. In the last section, we discuss and summarize the main findings.

2 Methodology and data

2.1 Vegetation biophysics

Here, we apply an off-line version of the vegetation model that has been implemented into a coupled global carbon-chemistry-climate model framework (Unger et al., 2013). The off-line model can be run at the site-level or in distributed mode for a designated region. The vegetation biophysics module computes the photosynthetic uptake of CO_2 coupled with the transpiration of water vapor at the 1 h physical integration time step of the off-line model. The vegetation biophysics calculates C3 and C4 photosynthesis using the well-established Michealis–Menten enzyme-kinetics leaf model of photosynthesis (Farquhar et al., 1980; von Caemmerer and Farquhar, 1981) and the stomatal conductance model of Ball and Berry (Collatz et al., 1991). The coupled photosynthesis/stomatal conductance leaf model has been widely used to project terrestrial biosphere responses to global change. The model is briefly summarized here for transparency and completeness. The leaf model assumes that the rate of net CO_2 assimilation (A_{net}) in the leaves of C3 and C4 plants is limited by one of three processes: (i) the capacity of the ribulose 1,5-bisphosphate (RuBP) carboxylase-oxygenase enzyme (Rubisco) to consume RuBP (J_c); (ii) the capacity of the Calvin cycle and the thylakoid reactions to regenerate RuBP supported by electron transport (J_e); (iii) the capacity of starch and sucrose synthesis to consume triose phosphates and regenerate inorganic phosphate for photo-phosphorylation in C3 and phosphoenolpyruvate (PEP) limitation in C4 (J_s). J_c, J_e, and J_s are described as functions of the maximum carboxylation capacity (V_{cmax}) at the optimal temperature, 25 °C, and the internal leaf CO_2 concentration

ACPD
13, 31563–31605, 2013

(C_i). The gross rate of carbon assimilation from photosynthesis (A) is given by:

$$A = \min(J_c, J_e, J_s) \quad (1)$$

Net carbon assimilation is given by:

$$A_{net} = A - R_d \quad (2)$$

where R_d is the rate of dark respiration:

$$R_d = 0.015 \cdot V_{cmax} \quad (3)$$

Leaf stomata control the uptake of CO_2 vs. the loss of H_2O. At equilibrium, the stomatal conductance of water vapor through the leaf cuticle (g_s in mol [H_2O] $m^{-2} s^{-1}$) depends on the net rate of carbon assimilation:

$$g_s = m\frac{A_{net} \cdot RH}{c_s} + b = \frac{1}{r_s} \quad (4)$$

where m and b are the slope and intercept derived from empirical fitting to the Ball and Berry stomatal conductance equations, RH is relative humidity, c_s is the CO_2 concentration at the leaf surface, and r_s is the stomatal resistance to water vapor. Appropriate photosynthesis parameters for the local vegetation type are taken from (Friend and Kiang, 2005) and the Community Land Model (Oleson et al., 2010) with updates from Bonan et al. (2011) (Table 1).

The canopy radiative transfer scheme assumes a closed canopy and layers the canopy for light stratification using an adaptive number of layers (typically 2–16) (Friend and Kiang, 2005). Each canopy layer distinguishes sunlit and shaded regions for which the direct and diffuse photosynthetically active radiation (PAR) is computed (Spitters et al., 1986). The coupled photosynthesis and stomatal conductance equations are solved analytically using a cubic function of A_{net}. C_i is calculated explicitly at the leaf level. Scaling of the leaf to canopy level is through stratification of canopy light levels and leaf area profiles. The photosynthetic uptake of CO_2 is accumulated into a carbon reserve pool, from which other processes may allocate uses.

ACPD
13, 31563–31605, 2013

2.1.1 O_3 damage effects to photosynthesis

O_3 oxidizes cellular membranes and photosynthetic tissues when it enters leaves through stomata, leading to reductions in photosynthesis and GPP. Since transpiration is closely related to the photosynthetic rate, O_3 also inhibits stomatal conductance. A semi-mechanistic parameterization is employed to estimate the O_3 damage effects to both photosynthesis and stomatal conductance (Sitch et al., 2007). The exposure to O_3 leads to a reduction in photosynthesis:

$$A' = F \cdot A_{\text{net}} \tag{5}$$

where F is the reduction fraction calculated as

$$F = 1 - a \cdot U_{>O_3T} \tag{6}$$

where a is the O_3 sensitivity coefficient derived from observations. Two cases are examined: high and low O_3 sensitivity following Sitch et al. (2007). $U_{>O_3T}$ is the instantaneous leaf uptake of O_3 flux above a plant function type (PFT)-specific threshold (Table 1),

$$U_{>O_3T} = \max\left[\left(F_{O_3} - O_3T\right), 0\right] \tag{7}$$

here F_{O_3} is the O_3 flux entering the leaf through the stomata,

$$F_{O_3} = \frac{[O_3]}{r_b + \kappa \cdot r'_s} \tag{8}$$

where $[O_3]$ is the O_3 concentration at the top of the canopy, r_b is the boundary layer resistance. The stomatal resistance to O_3 is calculated based on stomatal resistance to water r_s with a ratio constant $\kappa = 1.67$. From Eq. (4), the decrease in A_{net} reduces the stomatal conductance g_s proportionally,

$$r'_s = \frac{1}{g'_s} = \frac{1}{F \cdot g_s} \tag{9}$$

ACPD
13, 31563–31605, 2013

The r'_s and g'_s are the O_3-damaged stomatal resistance and conductance, respectively. When the plant is exposed to [O_3] (Eq. 8), the excess O_3 flux entering leaves (Eq. 7) causes $F < 1$ (Eq. 6), decreasing A_{net} (Eq. 5) while increasing the stomatal resistance (Eq. 9). The latter will act to reduce the O_3 uptake flux (Eq. 8) to protect the plant. Thus, the scheme considers associated changes in both photosynthetic rate and stomatal conductance. When photosynthesis is inhibited by O_3, the stomatal conductance decreases accordingly to resist more air passing through the stomata, resulting in a decline of the oxidant fluxes inside leaves, as described through Eqs. (5)–(9). Consequently, this coupled scheme represents the equilibrium state between the CO_2 demand for vegetation growth and the protection against O_3 damage by plant. Although some studies suggest a decoupling between photosynthesis and stomatal conductance (e.g. Lombardozzi et al., 2012a, b), the Sitch et al. (2007) scheme shows a promising application in global climate-chemistry-carbon models and is well validated with field measurements for our simulations.

2.1.2 Vegetation structure

The vegetation model simulates eight PFTs, using either C3 or C4 photosynthesis (Table 1). We apply two different sets of land cover and leaf area index (LAI) in the simulations. The first one is the PFT-specified vegetation cover fraction and LAI retrieved by the Moderate Resolution Imaging Spectroradiometer (MODIS, Knyazikhin et al., 1998), which is interpolated from monthly to daily values. The other one uses LAI from the Global Modeling and Assimilation Office (GMAO) Modern Era-Retrospective Analysis (MERRA) dataset. The MERRA LAI is assimilated based on radiance data retrieved by over 20 satellites (Rienecker et al., 2011). It is available on daily scale from 1980 onwards, but has no PFT-specified information. We assign the MERRA LAI to a specific model PFT based on biome type at one site or the land cover determined by the International Satellite Land-Surface Climatology Project (ISLSCP, Hall et al., 2006) at grid squares.

ACPD
13, 31563–31605, 2013

2.1.3 Meteorological Forcing

For the site-level simulation, we use hourly in situ measurements of surface meteorological variables, including surface air temperature, specific humidity, wind speed, surface pressure, and CO_2 concentrations. We gap-fill the site-based observations with that from the MERRA-land data (Reichle et al., 2011), which is interpolated to each site based on the site location. By default the distributed off-line model uses hourly MERRA-land data. The original resolution of $0.5^\circ \times 0.667^\circ$ by latitude and longitude is degraded to $1^\circ \times 1.333^\circ$ due to current disk space limitation. We apply the surface climatic variables (surface air temperature, specific humidity, wind speed, surface pressure, precipitation, direct PAR, and diffuse PAR), and soil variables at 6 depths (soil temperature and soil moisture).

2.1.4 Surface [O_3]

Hourly and daily maximum 8 h average surface [O_3] representative of the present day climate ($\sim$ 2005) are taken from previous simulations using NASA Model-E2 (Shindell et al., 2013). The model resolution is $2^\circ \times 2.5^\circ$ latitude by longitude horizontal resolution with 40-vertical layers extending to 0.1 hPa. The gas-phase chemistry and aerosol modules are fully integrated, so that these components interact with each other and with the physics of the climate model (Bell et al., 2005; Shindell et al., 2006; Unger, 2011; Shindell et al., 2013). The model surface O_3 is validated using measurements from 73 Clean Air Status and Trends Network (CASTNET) sites operated by the Unitied States Environmental Protection Agency (EPA) (http://epa.gov/castnet/javaweb/ozone.html) and $\sim$ 1200 monitor sites managed by the EPA AIRDATA (http://www.epa.gov/airdata/). These sites are operated on the county level scale. The CASTNET provides hourly [O_3] at rural sites from 1996–2005. The AIRDATA network provides daily maximum 8 h average (MDA8) [O_3], covering both urban and rural regions. We use AIRDATA data for the year 2005.

ACPD
13, 31563–31605, 2013

2.2 Simulations

2.2.1 Site-level runs

We configure a site level version of the model for the 40 eddy covariance flux tower sites described in detail in the NACP synthesis (Schaefer et al., 2012, Appendix Table A). In these simulations, the model is driven with the local meteorology and radiation data measured at the towers where available and gap-filled with the GMAO MERRA reanalysis data where data are not available. The MERRA meteorological forcings are interpolated to each site based on the site location (Fig. 1). Measurements are available for a wide range of time periods across the different sites ranging from the minimum of 1 yr at Fermi Lab (US-IB1) and the maximum of 15 yr at Harvard Forest (US-HA1). Measurement sites cover a range of different vegetation types including: evergreen needleleaf forest, deciduous broadleaf forest, grasslands, croplands, closed shrublands, mixed forests, permanent wetlands, and woody savannas. Table 2 summarizes how the NACP vegetation types are mapped onto the 8 model PFTs.

A further four simulations are carried out at each site, based on the different combinations of meteorological and vegetation forcings, to assess the sensitivity of the results to local vs. renalaysis meterological forcing and LAI (Table 3). Two, MERRA_MODIS and MERRA_VEG, use hourly meteorology from MERRA-land reanalyses alone. The other two, SITEM_MODIS and SITEM_VEG, use site-based measurements with gap-filled MERRA reanalysis. Simulations use 2 datasets of LAI: (1) MERRA_VEG and SITEM_VEG use LAI from the MERRA-land reanalyses, which provide non PFT-specified LAI that we assign to the specific biome type at each site (Table A), while (2) MERRA_MODIS and SITEM_MODIS use PFT-specified LAI retrieved by the MODIS. We perform two additional site-level simulations, which use the same forcings as that for SITEM_VEG but with the impact of O_3 uptake on photosynthesis. These two experiments, SITEM_VEG_HO3 and SITEM_VEG_LO3, use either high or low O_3 sensitivity as defined by the coefficient *a* in Table 1.

ACPD
13, 31563–31605, 2013

2.2.2 Distributed run over US region

A gridded version of the vegetation model at $1^{\circ} \times 1.333^{\circ}$ latitude by longitude horizontal resolution for the US region is driven with MERRA meteorological forcings for the period 1998–2007. In the distributed model, vegetation cover types are from the ISLSCP and LAI is form the MERRA-land reanalysis. We assign the MERRA LAI to the corresponding PFT types defined by ISLSCP (Fig. 2), which may be inconsistent with that from NACP sites (Fig. 1). The 18 ISLSCP land types are converted to 8 PFTs used in the model (Table 2). In contrast to the site-level simulations that assume C4 photosynthesis for cropland sites, which mainly grow maize (Schaefer et al., 2012), the regional simulation assumes C3 photosynthesis for cropland. At large scales, C3 and C4 crops are usually mixed and most of US crops are C3. We carry out 2 simulation cases with high and low O_3 damage sensitivity.

3 Results

3.1 Evaluation of GPP at NACP sites

Figure 3 compares daily LAI from MERRA and MODIS at each NACP site. The two datasets show similar annual cycles at most evergreen and deciduous sites. However, the MERRA LAI at grasslands and croplands is near zero during cold seasons while the MODIS is positive all year round. In addition, the two LAIs show different seasonality at shrubland sites, such as US-SO2 and US-Ton. Later analyses reveal that simulated GPP with MERRA LAI has much lower biases relative to that with MODIS LAI.

Figure 4 shows GPP from observations and simulations of SITEM_VEG for individual NACP sites. The simulations capture the magnitude and seasonality of GPP for most sites. We calculate a correlation coefficient of 0.67 between simulations and observations for the annual mean GPP at these sites. The correlation is higher at 0.8 for summer. On average, the annual GPP is 3.8 $g C m^{-2} day^{-1}$, 27 % higher than the

ACPD
13, 31563–31605, 2013

3.0 g C m^{-2} day^{-1} observed at these sites. The inclusion of O_3 damage effects improves simulations at some sites, especially the croplands, such as US-Ne2 and US-Ne3.

To quantify the performance of vegetation model, we estimate the χ^2 for each site following the method described in Schaefer et al. (2012),

$$\chi^2 = \frac{1}{n}\sum_{i=1}^{n}\left(\frac{r_i}{\sigma_i}\right)^2 \quad (10)$$

where

$$r_i = (\mathrm{GPP}_{si} - \mathrm{GPP}_{oi}) \quad (11)$$

is the difference between the pair of simulation and observation. σ_i is the observational uncertainties. n is the length of observations. The lower the χ^2, the smaller the model biases. If $\chi^2 < 1$, the simulation bias is on average smaller than the measurement uncertainty, indicating a good performance of the model. Here, we define a reasonable performance of $\chi^2 < 4$, when the residual is less than twice the measurement uncertainty.

Figure 5a shows the sorted χ^2 values at NACP sites. Among the 40 sites, 23 have reasonable performance with $\chi^2 < 4$. The simulation is the best ($\chi^2 < 1$) at site US-Ne1, which is C4 cropland (Fig. 4). Simulations at other crop sites, US-IB1, US-Ne2, and US-Ne3, have low biases as well. For the 23 sites with low χ^2, 12 are based in needleleaf forests. These sites usually have multiple years of measurements and provide good samples for testing the consistency between simulations and observations. Simulations at 4 broadleaf forest and 3 shrubland sites have $\chi^2 < 4$, and the latter usually has low GPP whose peak is not higher than 10 g C m^{-2} day^{-1} (Fig. 4).

On the other hand, 17 sites have poor simulations ($\chi^2 > 4$). Among them, 8 are needleleaf forests, 2 are broadleaf forests, and 2 are shrubland. The common feature of the biases in these sites is the overestimation of peak GPP during summer (Fig. 4). The possible cause is that we use uniform photosynthesis parameters for one PFT

ACPD
13, 31563–31605, 2013

in the vegetation model, disregarding the influences of tree speciation and age. The simulations, however, are poor at all 5 grassland sites. The biases in these sites are due to the mismatch of GPP seasonality (Fig. 4). It indicates that the remote sensing LAI may not represent local changes in plant growth and phenology, especially for vegetation types with low biomass. In addition, the model is unable to resolve the GPP variability for sites in close proximity. For example, sites CA-SJ1, CA-SJ2, and CA-SJ3 are located close to each other. Simulations at these sites have similar magnitude in simulated GPP while observations show distinct variability between the sites.

Figure 6 compares average χ^2 for the different sensitivity experiments. Since simulations at four sites, CA-Let, US-Var, CA-SJ1, and CA-SJ2, have excessive biases (Fig. 5a), we exclude them from statistics in the following discussion. As Fig. 6 shows, the χ^2 decreases from experiment 1 to 4, indicating enhanced simulation performance due to the improved forcings. Inclusion of site forcings in the simulation only slightly improves the model performance, relative to those with MERRA forcing alone because the variables provided by sites are not complete for the vegetation model and the MERRA meteorology is used to gap-fill. Compared with changes in input meteorology, the choice of LAI forcing has more significant impacts on the simulation. The model has $\chi^2 > 10$ with MODIS vegetation cover and LAI (MODIS LAI is PFT-specific but may not be consistent with the land types as described by NACP sites). When driving with MERRA LAI for the consistent PFTs, the χ^2 values show reductions of ~ 5 for different meteorological forcings. Such results are consistent with conclusions by Desai et al. (2008) and Puma et al. (2013), which showed that biological and phenological factors are more important than meteorological ones in controlling the terrestrial carbon exchange.

3.2 Evaluation of modeled surface [O_3]

We validate summertime surface O_3 simulated by the NASA Model-E2 chemistry-climate model with observations from the CASTNET and AIRDATA (Fig. 7). High O_3 level appears in the Eastern US due to anthropogenic emissions and in the mountain-

ACPD
13, 31563–31605, 2013

ous West due to high elevation. The model generally captures this spatial pattern with a correlation coefficient of 0.39 against observations over the selected 73 CASTNET sites (Figs. 7a and b). The simulation overestimates the O_3 level by 4 ppbv (12 %) in the East and 1 ppbv (3 %) in the West. The CASTNET sites are located in rural sites, which usually have lower [O_3] than that in urban areas, except for some megacities where the excessive NO_x emissions result in lower O_3 level (Gregg et al., 2003). As a result, we compare the simulated MDA8 [O_3] with monitored at ~ 1200 AIRDATA sites, which covers both urban and rural regions (Fig. 7c). In the East, the model captures high [O_3] centers around Michigan, Indiana, and Ohio states and that along the northeast coast. In the West, the simulation reproduces high [O_3] at mountains and that in California. On average, the simulated MDA8 [O_3] is lower by 0.5 ppbv (1 %) in the East and 3.5 ppbv (7 %) in the West. The correlation coefficient between simulations and observations is as high as 0.51 (Fig. 7d).

3.3 O_3 damage effects at NACP sites

The NACP sites do not monitor [O_3] and the simulated O_3 is applied to quantify its damage effect to GPP. The summer average [O_3] are 30–50 ppbv at 24 US sites (Fig. 8a). The damage effect is the strongest at 4 crop sites, US-Ne1, US-IB1, US-Ne2, and US-Ne3, where the reductions in GPP are 10–16 % depending on the low or high O_3 sensitivity. The average [O_3] at these sites are only 32 ppbv, much lower than that for other PFTs. However, the O_3-free GPP at these sites are the largest among the all 24 sites (Fig. 8b), indicating high stomatal conductance and O_3 flux entering the plant. The higher O_3 sensitivity of crops relative to other PFTs results in stronger damage effects (Table 1). On the other hand, the lowest reduction of 1–2 % appears in 3 shrub sites, US-Ton, US-SO2, and US-Los, although mean [O_3] there are as high as 43 ppbv. The main reason for the slight damage is the low stomatal conductance connected to the small GPP (Fig. 8b). For the same reason, the damage for C3 grass is as low as 1–2 %, although the GPP of this plant is very sensitive to O_3 (Table 1). For needleleaf and

ACPD
13, 31563–31605, 2013

broadleaf forest sites, the O_3 damage effects are estimated to be 2–5 % and 3–9 %, because the latter has double O_3 sensitivity compared with the former.

We compare the simulated O_3 damage effect with measurements from literature. Site-based experiments usually have different $[O_3]$ from the ambient level we used, making the validation difficult. As a result, we perform 14 additional sensitivity simulations for each of NACP sites. All tests use meteorological and vegetation forcings the same as SITEM_VEG (Table 3), except for the different $[O_3]$ and O_3 sensitivity. These experiments are divided into two groups, 7 in each, using either low or high O_3 sensitivity. In each group, simulations are performed with constant $[O_3]$ at 20, 40, 60, 80, 100, 120, 140 ppbv, respectively. Figure 9 presents the changes in GPP for all and individual PFTs in the presence of different $[O_3]$. The reductions in GPP are greater with the increase of the $[O_3]$. For a given $[O_3]$, the O_3 damage effect is strongest for C4 crops but weakest for shrubland. Compared with the meta-analyses of Wittig et al. (2007) and Lombardozzi et al. (2013), the simulations show reasonable reductions in GPP by O_3 for forests and most other model PFTs. Studies in shrubland are limited. Zhang et al. (2012) investigated the responses of four shrub species to $[O_3] = 70$ ppbv and found reductions in net photosynthesis by 50–60 %. However, the average net photosynthesis (A_{net}) of these species is 8–16 g [C] $m^{-2} s^{-1}$, much higher than the gross photosynthesis (A) of 6 g [C] $m^{-2} s^{-1}$ at NACP sites, likely because the latter are located at dry and/or cold areas (Fig. 1). For grass and crop sites, comparison with observations is more complex. Leisner et al. (2012) showed that the yield and growth responses of C3 and C4 plants to O_3 are similar. Since the O_3 damage is very dependent on the magnitude of original GPP, we attribute one measurement with grass/crops to a C3 group if the plant shows low O_3-free GPP or to a C4 group if original GPP is high. For example, rice is a C3 plant by nature, however, experiments by Ishii et al. (2004) show original GPP of ~ 14 g [C] $m^{-2} s^{-1}$, double that of 7 g [C] $m^{-2} s^{-1}$ for C3 grass sites but close to the 16 g [C] $m^{-2} s^{-1}$ for C4 crop sites in our simulation. In this case, we compare results from Ishii et al. (2004) with simulations at C4 crop sites. The comparison

ACPD
13, 31563–31605, 2013

in Fig. 9 show that responses of C3 grass may be underestimated by 30 % while that of C4 crops are reasonable.

Inclusion of O_3 damage effect improves the site-level simulations (Figs. 5b and c). For most sites, the χ^2 of simulated GPP decreases when considering vegetation responses to O_3, and the improvement is better when higher O_3 sensitivity is applied. At these sites, the reduced GPP at peak seasons is closer to measurements (Fig. 4), leading to smaller biases for simulations. This is the case even for the sites where the original $\chi^2 < 2$, such as US-Ne1, US-IB1, and US-Ne2. As a result, the average χ^2 decreases by 3–8 %, depending on the O_3 sensitivity in the simulation (Fig. 6). Finally, the simulated annual GPP averaged over all NACP sites changes from 3.8 $g C m^{-2} day^{-1}$ to 3.6 $g C m^{-2} day^{-1}$ with the high O_3 sensitivity simulation case, closer to the observations of 3.0 $g C m^{-2} day^{-1}$.

3.4 O_3 vegetation damage effect on GPP in US region

Figure 10 shows the summer GPP in US simulated with gridded MERRA forcing. High values of GPP appear East of 95° W, because the land there is covered by crops and forests. In the West, however, the coverage of grass and shrub and the low water availability (low precipitation and soil moisture) over semi-arid regions lead to low carbon assimilation rate. This spatial pattern matches the distribution of NACP site-level flux (Fig. 10a), with a correlation coefficient of 0.49 for 32 sites below 50° N (Fig. 10b). However, this correlation is lower than the 0.69 estimated for site-level simulation SITEM_VEG at the same sites and the same season. Since the meteorological forcings and LAI are similar, the difference in land cover, ISLSCP vs. site definitions, accounts for the discrepancy between regional and site-level simulations.

On average, the summer GPP is 9.1 $g C m^{-2} day^{-1}$ in the East and 3.7 $g C m^{-2} day^{-1}$ in the West, giving a mean value of 5.9 $g C m^{-2} day^{-1}$ for US The gross carbon uptake is estimated to be 4.26 ± 0.16 Pg C for the summer, accounting for 55–58 % of the annual average value of 7.48 ± 0.25 Pg C over the 1998–2007 period. Our estimate of annual

ACPD
13, 31563–31605, 2013

uptake is consistent with previous literature. For example, Xiao et al. (2010) upscaled site-level GPP flux to continental scale with a regression tree approach based on both the NACP flux and the remote-sensing variables. They estimated that the total GPP in US ranges from 6.91 to 7.33 $Pg\,C\,yr^{-1}$ during 2000–2006. Using the same observations but with a process-based biogeochemical model, Chen et al. (2011) achieved a range of 7.02–7.78 $Pg\,C\,yr^{-1}$ for 2000–2005, which is even closer to our estimate.

Figure 11 shows the O_3 vegetation damage effect in US Due to the consistently high values of both GPP and [O_3], mean reductions of 3–7 % in summer GPP are predicted in the East, depending on the O_3 sensitivity applied in the simulations. Regionally, reduction fraction reaches as high as 13–17 % in areas with high [O_3], such as Michigan, Indiana, Ohio, and states along the northeast coast. O_3 damage effects in central US cropland are not as severe in the distributed vs. site level model because the distributed model assumes C3 photosynthesis for crops, resulting in lower original GPP relative to NACP crop sites. Despite high surface [O_3] over mountainous elevated areas in the West (Fig. 7), impacts on GPP are limited due to low stomatal conductance determined by the low photosynthetic rate there (Fig. 10a). The Pacific northwestern forests are an exception. On average, the total summer GPP is reduced by 2–5 % by O_3 damage effects in the West. A similar reduction fraction is predicted for the annual GPP.

Felzer et al. (2004) previously found annual average O_3-induced NPP reductions of 2.6–6.8 % over US for 1989–1993 and simulated the largest reductions in states close to the Great Lakes and along the Eastern coast, where the high O_3 sensitivity of crops makes the dominant contribution. Our study examines O_3 damage effects a decade later than Felzer et al. (2004) but gives consistent impact values, which we attribute to offsetting influences of (i) surface O_3 reductions due to air quality control legislation (Bloomer et al., 2010) and (ii) GPP increases due to CO_2-fertilization and rising temperatures (Keenan et al., 2013). Felzer et al. (2004) estimated a maximum local NPP reduction of 34 %, which is double the maximum of 17 % in our analyses. Furthermore, Felzer et al. (2004) found widespread reductions of > 6 % in the Midwest where there is almost no O_3 impact in this study (Fig. 11). The most likely explanation for the dis-

ACPD
13, 31563–31605, 2013

crepancy is the different vegetation cover datasets and vegetation type classification used in each study.

Surface [O_3] continues to exhibit a decreasing trend over the past 2 decades, especially in the East, mainly due to precursor emission controls (Lefohn et al., 2010). The community debates how surface [O_3] will respond to future emissions and climate change. On the one hand, surface [O_3] may decline by the mid 21st century due to large reductions in regional anthropogenic precursor emissions (Wu et al., 2008). On the other hand, climate change effects alone may increase local surface [O_3] due to the warmer, drier, and more stable environment (Leibensperger et al., 2008; Wu et al., 2008). Due to the uncertainty in future surface [O_3] projections, our strategy here is to perform four additional sensitivity experiments with ±25 % changes in [O_3] for each O_3 sensitivity case. Figure 12 shows that [O_3] increases of 25 % may reduce GPP in the eastern US by 6–11 %, with a maximum local reduction of 26 % in the high O_3 sensitivity case. The damage magnitude with low O_3 sensitivity (Fig. 12b) mimics the present-day estimate with high O_3 sensitivity (Fig. 11b). In contrast, the O_3 damage to the eastern GPP is as low as 1–3 %, when [O_3] decreases by 25 % (Fig. 12a and c), indicating a promising consequence to ecosystem-health of O_3 precursor emissions control.

4 Discussion and conclusions

We performed an up-to-date estimate of O_3 vegetation damage effects on GPP in the US during 1998–2007. The semi-mechanistic parameterization of O_3 inhibition on photosynthesis proposed by Sitch et al. (2007) was implemented into a process-based vegetation model. We evaluated the simulated GPP with in situ measurements from 40 NACP sites. The simulation captures the seasonality and interannual variability of GPP at most sites and yields a correlation coefficient of 0.67 for the annual mean GPP with observations. The model biases are the lowest for cropland sites but the highest at grassland sites, because the simulation exhibits incorrect seasonality for the latter.

ACPD
13, 31563–31605, 2013

Model GPP is sensitive to choice of vegetation forcings, including the biome types and the LAI. The simulations with MERRA LAI assigned to site-specific PFT show much lower biases relative to the ones with PFT-specified LAI retrieved by the MODIS.

We applied hourly surface O_3 simulated by a global chemistry-climate model. The summertime average [O_3] from the global chemistry-climate model has a correlation coefficient of 0.39 with observations from 73 CASTNET sites. In addition, the MDA8 [O_3] correlates with measurements at ~ 1200 AIRDATA sites, which cover both urban and rural sites, as high as $R = 0.51$. In response to the ambient [O_3] of 30–50 ppbv, GPP decreases by 1–16 % at NACP sites, depending on the O_3 sensitivity and biome types. The magnitude of the GPP reduction is directly related to the rate of photosynthesis. Maximum reductions of 10–16 % occur in cropland and the minimum reductions of only 1–2 % occur in shrubland. The simulated O_3 damage effects are consistent with laboratory and field measurements reported in previous literature. Inclusion of the O_3 inhibition effect improves the simulated annual average GPP at NACP sites from 3.8 g C m^{-2} day^{-1} to 3.6 g C m^{-2} day^{-1} to more closely match the observational average of 3.0 g C m^{-2} day^{-1}.

We performed regional simulations for the US with gridded MERRA forcing and land cover from the ISLSCP. Generally, GPP is higher in the eastern than the western US as a result of the vegetation distribution. Summertime average GPP is 5.9 g C m^{-2} day^{-1} for the entire US region (9.1 g C m^{-2} day^{-1} in the east and 3.7 g C m^{-2} day^{-1} in the west). The total carbon uptake was estimated to be 4.26 ± 0.16 Pg C for the summer, accounting for 55–58 % of the annual value of 7.48 ± 0.25 Pg C over the 1998–2007 period. In the presence of O_3, the total carbon uptake decreases by 3–7 % in the East, with maximum reductions of 13–17 % in states close to the Great Lakes and along the eastern coast. Sensitivity tests show that the average O_3 damage to GPP is only 1–3 %, when [O_3] decreases by 25 %.

The main limitations of this study are that we did not account for various biosphere-atmosphere interactions in the model simulations. For instance, a possible negative feedback from plant isoprene emission (an important O_3 precursor) may dampen the

ACPD
13, 31563–31605, 2013

O_3 damage effect to a certain extent (Unger et al., 2013). GPP reductions imply higher atmospheric CO_2 concentration, which may result in temperature and precipitation changes on both regional and global scales. In addition, the decreased stomatal conductance may inhibit evapotranspiration (Bernacchi et al., 2007), leading to consequent changes in canopy temperature, precipitation, soil moisture, and other surface hydrological and meteorological parameters. Conversely, emerging research has found that the O_3 vegetation damage effects can actually result in a loss of plant stomatal control, and a consequent decoupling of the stomatal response from photosynthesis inhibition (Lombardozzi et al., 2012a, b). The O_3 vegetation damage may lead to inhibition of stomatal response to other environmental drivers, including drought stress (Uddling et al., 2009). For example, exposure of forest ecosystems to enhanced ambient O_3 in the southeast US resulted in increased transpiration, water-use and a resultant decrease in streamflow (Sun et al., 2012). In a grassland ecosystem, an O_3-induced increase in stomatal conductance was shown to result in an increase in stomatal O_3 flux into the plant (Hayes et al., 2012). All of these feedbacks may influence both surface $[O_3]$ and carbon assimilation rate with currently uncertain magnitude. In future work, our goal is to quantify the O_3 damage effects on the carbon cycle interactively, including decoupled photosynthesis and stomatal conductance, using the Yale-E2 global carbon-climate-chemistry model.

Acknowledgements. Data for this analysis was provided by the North American Carbon Program Site Synthesis. Funding for this research was provided by Yale University. This project was supported in part by the facilities and staff of the Yale University Faculty of Arts and Sciences High Performance Computing Center.

References

Ainsworth, E. A., Yendrek, C. R., Sitch, S., Collins, W. J., and Emberson, L. D.: The Effects of tropospheric ozone on net primary productivity and implications for climate change, Annu. Rev. Plant Biol., 63, 637–661, doi:10.1146/Annurev-Arplant-042110-103829, 2012.

ACPD
13, 31563–31605, 2013

Barr, A., Ricciuto, D., Schaefer, K., Richardson, A., Agarwal, D., Thornton, P., Davis, K., Jackson, B., Cook, R., Hollinger, D., Ingen, C. v., Amiro, B., Andrews, A., Arain, M., Baldocchi, D., Black, T., Bolstad, P., Curtis, P., Desai, A., Dragoni, D., Flanagan, L., Gu, L., Katul, G., Law, B., Lafleur, P., Margolis, H., Matamala, R., Meyers, T., McCaughey, H., Monson, R., Munger, J., Oechel, W., Oren, R., Roulet, N., Torn, M., and Verma, S.: NACP Site: Tower Meteorology, Flux Observations with Uncertainty, and Ancillary Data, Oak Ridge National Laboratory Distributed Active Archive Center, Oak Ridge, Tennessee, USA, 2013.

Bell, N., Koch, D., and Shindell, D. T.: Impacts of chemistry-aerosol coupling on tropospheric ozone and sulfate simulations in a general circulation model, J. Geophys. Res., 110, D14305, doi:10.1029/2004jd005538, 2005.

Bernacchi, C. J., Kimball, B. A., Quarles, D. R., Long, S. P., and Ort, D. R.: Decreases in stomatal conductance of soybean under open-air elevation of [CO_2] are closely coupled with decreases in ecosystem evapotranspiration, Plant Physiol., 143, 134–144, doi:10.1104/Pp.106.089557, 2007.

Bloomer, B. J., Vinnikov, K. Y., and Dickerson, R. R.: Changes in seasonal and diurnal cycles of ozone and temperature in the eastern US, Atmos. Environ., 44, 2543–2551, doi:10.1016/J.Atmosenv.2010.04.031, 2010.

Bonan, G. B., Lawrence, P. J., Oleson, K. W., Levis, S., Jung, M., Reichstein, M., Lawrence, D. M., and Swenson, S. C.: Improving canopy processes in the Community Land Model version 4 (CLM4) using global flux fields empirically inferred from FLUXNET data, J. Geophys. Res., 116, G02014, doi:10.1029/2010jg001593, 2011.

Chen, M., Zhuang, Q., Cook, D. R., Coulter, R., Pekour, M., Scott, R. L., Munger, J. W., and Bible, K.: Quantification of terrestrial ecosystem carbon dynamics in the conterminous United States combining a process-based biogeochemical model and MODIS and AmeriFlux data, Biogeosciences, 8, 2665–2688, doi:10.5194/bg-8-2665-2011, 2011.

Collatz, G. J., Ball, J. T., Grivet, C., and Berry, J. A.: Physiological and environmental-regulation of stomatal conductance, photosynthesis and transpiration – a model that includes a laminar boundary-layer, Agr. Forest Meteorol., 54, 107–136, doi:10.1016/0168-1923(91)90002-8, 1991.

Cooper, O. R., Parrish, D. D., Stohl, A., Trainer, M., Nedelec, P., Thouret, V., Cammas, J. P., Oltmans, S. J., Johnson, B. J., Tarasick, D., Leblanc, T., McDermid, I. S., Jaffe, D., Gao, R., Stith, J., Ryerson, T., Aikin, K., Campos, T., Weinheimer, A., and Avery, M. A.: Increasing

ACPD
13, 31563–31605, 2013

springtime ozone mixing ratios in the free troposphere over western North America, Nature, 463, 344–348, doi:10.1038/Nature08708, 2010.
Desai, A. R., Noormets, A., Bolstad, P. V., Chen, J. Q., Cook, B. D., Davis, K. J., Euskirchen, E. S., Gough, C. M., Martin, J. G., Ricciuto, D. M., Schmid, H. P., Tang, J. W., and Wang, W. G.: Influence of vegetation and seasonal forcing on carbon dioxide fluxes across the Upper Midwest, USA: implications for regional scaling, Agr. Forest Meteorol., 148, 288–308, doi:10.1016/J.Agrformet.2007.08.001, 2008.
Farquhar, G. D., Caemmerer, S. V., and Berry, J. A.: A biochemical-model of photosynthetic CO_2 assimilation in leaves of C-3 species, Planta, 149, 78–90, doi:10.1007/Bf00386231, 1980.
Felzer, B., Kicklighter, D., Melillo, J., Wang, C., Zhuang, Q., and Prinn, R.: Effects of ozone on net primary production and carbon sequestration in the conterminous United States using a biogeochemistry model, Tellus B, 56, 230–248, doi:10.1111/J.1600-0889.2004.00097.X, 2004.
Felzer, B., Reilly, J., Melillo, J., Kicklighter, D., Sarofim, M., Wang, C., Prinn, R., and Zhuang, Q.: Future effects of ozone on carbon sequestration and climate change policy using a global biogeochemical model, Climatic Change, 73, 345–373, doi:10.1007/S10584-005-6776-4, 2005.
Feng, Z. Z., Kobayashi, K., and Ainsworth, E. A.: Impact of elevated ozone concentration on growth, physiology, and yield of wheat (*Triticum aestivum L.*): a meta-analysis, Glob. Change Biol., 14, 2696–2708, doi:10.1111/J.1365-2486.2008.01673.X, 2008.
Friend, A. D. and Kiang, N. Y.: Land surface model development for the GISS GCM: effects of improved canopy physiology on simulated climate, J. Climate, 18, 2883–2902, doi:10.1175/Jcli3425.1, 2005.
Goodale, C. L., Apps, M. J., Birdsey, R. A., Field, C. B., Heath, L. S., Houghton, R. A., Jenkins, J. C., Kohlmaier, G. H., Kurz, W., Liu, S. R., Nabuurs, G. J., Nilsson, S., and Shvidenko, A. Z.: Forest carbon sinks in the Northern Hemisphere, Ecol. Appl., 12, 891–899, doi:10.2307/3060997, 2002.
Gregg, J. W., Jones, C. G., and Dawson, T. E.: Urbanization effects on tree growth in the vicinity of New York City, Nature, 424, 183–187, doi:10.1038/Nature01728, 2003.
Hall, F. G., de Colstoun, E. B., Collatz, G. J., Landis, D., Dirmeyer, P., Betts, A., Huffman, G. J., Bounoua, L., and Meeson, B.: ISLSCP Initiative II global data sets: Surface boundary conditions and atmospheric forcings for land-atmosphere studies, J. Geophys. Res., 111, D22S01, doi:10.1029/2006JD007366, 2006.

ACPD
13, 31563–31605, 2013

Hayes, F., Wagg, S., Mills, G., Wilkinson, S., and Davies, W.: Ozone effects in a drier climate: implications for stomatal fluxes of reduced stomatal sensitivity to soil drying in a typical grassland species, Glob. Change Biol., 18, 948–959, doi:10.1111/J.1365-2486.2011.02613.X, 2012.

Hollaway, M. J., Arnold, S. R., Challinor, A. J., and Emberson, L. D.: Intercontinental transboundary contributions to ozone-induced crop yield losses in the Northern Hemisphere, Biogeosciences, 9, 271–292, doi:10.5194/bg-9-271-2012, 2012.

Huntingford, C., Cox, P. M., Mercado, L. M., Sitch, S., Bellouin, N., Boucher, O., and Gedney, N.: Highly contrasting effects of different climate forcing agents on terrestrial ecosystem services, Philos. T. R. Soc. A, 369, 2026–2037, doi:10.1098/Rsta.2010.0314, 2011.

Huntzinger, D. N., Post, W. M., Wei, Y., Michalak, A. M., West, T. O., Jacobson, A. R., Baker, I. T., Chen, J. M., Davis, K. J., Hayes, D. J., Hoffman, F. M., Jain, A. K., Liu, S., McGuire, A. D., Neilson, R. P., Potter, C., Poulter, B., Price, D., Raczka, B. M., Tian, H. Q., Thornton, P., Tomelleri, E., Viovy, N., Xiao, J., Yuan, W., Zeng, N., Zhao, M., and Cook, R.: North American Carbon Program (NACP) regional interim synthesis: terrestrial biospheric model intercomparison, Ecol. Model, 232, 144–157, doi:10.1016/J.Ecolmodel.2012.02.004, 2012.

Ishii, S., Marshall, F. M., and Bell, J. N. B.: Physiological and morphological responses of locally grown Malaysian rice cultivars (*Oryza sativa L.*) to different ozone concentrations, Water Air Soil Poll., 155, 205–221, doi:10.1023/B:Wate.0000026528.86641.5b, 2004.

Jaffe, D. and Ray, J.: Increase in surface ozone at rural sites in the western US, Atmos. Environ., 41, 5452–5463, doi:10.1016/J.Atmosenv.2007.02.034, 2007.

Karnosky, D. F., Skelly, J. M., Percy, K. E., and Chappelka, A. H.: Perspectives regarding 50 years of research on effects of tropospheric ozone air pollution on US forests, Environ. Pollut., 147, 489–506, doi:10.1016/J.Envpol.2006.08.043, 2007.

King, A. W., Hayes, D. J., Huntzinger, D. N., West, T. O., and Post, W. M.: North American carbon dioxide sources and sinks: magnitude, attribution, and uncertainty, Front. Ecol. Environ., 10, 512–519, doi:10.1890/120066, 2012.

Keenan, T. F., Hollinger, D. Y., Bohrer, G., Dragoni, D., Munger, J. W., Schmid, H. P., and Richardson, A. D.: Increase in forest water use efficiency as atmospheric CO_2 concentrations rise, Nature, 499, 324–327, doi:10.1038/nature12291, 2013.

Knyazikhin, Y., Martonchik, J. V., Myneni, R. B., Diner, D. J., and Running, S. W.: Synergistic algorithm for estimating vegetation canopy leaf area index and fraction of absorbed photosyn-

ACPD
13, 31563–31605, 2013

thetically active radiation from MODIS and MISR data, J. Geophys. Res., 103, 32257–32275, doi:10.1029/98jd02462, 1998.
Lefohn, A. S., Shadwick, D., and Oltmans, S. J.: Characterizing changes in surface ozone levels in metropolitan and rural areas in the United States for 1980–2008 and 1994–2008, Atmos. Environ., 44, 5199–5210, doi:10.1016/J.Atmosenv.2010.08.049, 2010.
Leibensperger, E. M., Mickley, L. J., and Jacob, D. J.: Sensitivity of US air quality to mid-latitude cyclone frequency and implications of 1980–2006 climate change, Atmos. Chem. Phys., 8, 7075–7086, doi:10.5194/acp-8-7075-2008, 2008.
Leisner, C. P. and Ainsworth, E. A.: Quantifying the effects of ozone on plant reproductive growth and development, Glob. Change Biol., 18, 606–616, doi:10.1111/J.1365-2486.2011.02535.X, 2012.
Levy, H., Schwarzkopf, M. D., Horowitz, L., Ramaswamy, V., and Findell, K. L.: Strong sensitivity of late 21st century climate to projected changes in short-lived air pollutants, J. Geophys. Res., 113, D06102, doi:10.1029/2007JD009176, 2008.
Lombardozzi, D., Levis, S., Bonan, G., and Sparks, J. P.: Predicting photosynthesis and transpiration responses to ozone: decoupling modeled photosynthesis and stomatal conductance, Biogeosciences, 9, 3113–3130, doi:10.5194/bg-9-3113-2012, 2012a.
Lombardozzi, D., Sparks, J. P., Bonan, G., and Levis, S.: Ozone exposure causes a decoupling of conductance and photosynthesis: implications for the Ball-Berry stomatal conductance model, Oecologia, 169, 651–659, doi:10.1007/S00442-011-2242-3, 2012b.
Lombardozzi, D., Sparks, J. P., and Bonan, G.: Integrating O_3 influences on terrestrial processes: photosynthetic and stomatal response data available for regional and global modeling, Biogeosciences, 10, 6815–6831, doi:10.5194/bg-10-6815-2013, 2013.
Oleson, K. W., Lawrence, D. M., Bonan, G. B., Flanne, M. G., Kluzek, E., Lawrence, P. J., Levis, S., Swenson, S. C., and Thornton, P. E.: Technical Description of version 4.0 of the Community Land Model (CLM), National Center for Atmospheric Research, Boulder, CONCAR/TN-478+STR, 2010.
Ollinger, S. V., Aber, J. D., and Reich, P. B.: Simulating ozone effects on forest productivity: Interactions among leaf-, canopy-, and stand-level processes, Ecol. Appl., 7, 1237–1251, doi:10.2307/2641211, 1997.
Pacala, S. W., Hurtt, G. C., Baker, D., Peylin, P., Houghton, R. A., Birdsey, R. A., Heath, L., Sundquist, E. T., Stallard, R. F., Ciais, P., Moorcroft, P., Caspersen, J. P., Shevliakova, E., Moore, B., Kohlmaier, G., Holland, E., Gloor, M., Harmon, M. E., Fan, S. M., Sarmiento, J. L.,

ACPD
13, 31563–31605, 2013

Goodale, C. L., Schimel, D., and Field, C. B.: Consistent land- and atmosphere-based US carbon sink estimates, Science, 292, 2316–2320, doi:10.1126/Science.1057320, 2001.
Pan, Y. D., Birdsey, R. A., Fang, J. Y., Houghton, R., Kauppi, P. E., Kurz, W. A., Phillips, O. L., Shvidenko, A., Lewis, S. L., Canadell, J. G., Ciais, P., Jackson, R. B., Pacala, S. W., McGuire, A. D., Piao, S. L., Rautiainen, A., Sitch, S., and Hayes, D.: A large and persistent carbon sink in the world's forests, Science, 333, 988–993, doi:10.1126/Science.1201609, 2011.
Puma, M. J., Koster, R. D., and Cook, B. I.: Phenological vs. meteorological controls on land-atmosphere water and carbon fluxes, J. Geophys. Res., 118, 14–29, doi:10.1029/2012jg002088, 2013.
Reichle, R. H., Koster, R. D., De Lannoy, G. J. M., Forman, B. A., Liu, Q., Mahanama, S. P. P., and Toure, A.: Assessment and enhancement of MERRA land surface hydrology estimates, J. Climate, 24, 6322–6338, doi:10.1175/Jcli-D-10-05033.1, 2011.
Ricciuto, D., Schaefer, K., Thornton, P., Davis, K., Cook, R., Liu, S., Anderson, R., Arain, M., Baker, I., Chen, J., Dietze, M., Grant, R., Izaurralde, C., Jain, A., King, A., Kucharik, C., Liu, S., Lokupitiya, E., Luo, Y., Peng, C., Poulter, B., Price, D., Riley, W., Sahoo, A., Tian, H., Tonitto, C., and Verbeeck, H.: NACP Site: Terrestrial Biosphere Model and Aggregated Flux Data in Standard Format, Oak Ridge National Laboratory Distributed Active Archive Center, Oak Ridge, Tennessee, USA, 2013.
Rienecker, M. M., Suarez, M. J., Gelaro, R., Todling, R., Bacmeister, J., Liu, E., Bosilovich, M. G., Schubert, S. D., Takacs, L., Kim, G. K., Bloom, S., Chen, J. Y., Collins, D., Conaty, A., Da Silva, A., Gu, W., Joiner, J., Koster, R. D., Lucchesi, R., Molod, A., Owens, T., Pawson, S., Pegion, P., Redder, C. R., Reichle, R., Robertson, F. R., Ruddick, A. G., Sienkiewicz, M., and Woollen, J.: MERRA: NASA's Modern-Era Retrospective Analysis for research and applications, J. Climate, 24, 3624–3648, doi:10.1175/Jcli-D-11-00015.1, 2011.
Rigby, M., Prinn, R. G., Fraser, P. J., Simmonds, P. G., Langenfelds, R. L., Huang, J., Cunnold, D. M., Steele, L. P., Krummel, P. B., Weiss, R. F., O'Doherty, S., Salameh, P. K., Wang, H. J., Harth, C. M., Muhle, J., and Porter, L. W.: Renewed growth of atmospheric methane, Geophys. Res. Lett., 35, L22805, doi:10.1029/2008GL036037, 2008.
Schaefer, K., Schwalm, C. R., Williams, C., Arain, M. A., Barr, A., Chen, J. M., Davis, K. J., Dimitrov, D., Hilton, T. W., Hollinger, D. Y., Humphreys, E., Poulter, B., Raczka, B. M., Richardson, A. D., Sahoo, A., Thornton, P., Vargas, R., Verbeeck, H., Anderson, R., Baker, I., Black, T. A., Bolstad, P., Chen, J. Q., Curtis, P. S., Desai, A. R., Dietze, M., Dragoni, D.,

ACPD
13, 31563–31605, 2013

Gough, C., Grant, R. F., Gu, L. H., Jain, A., Kucharik, C., Law, B., Liu, S. G., Lokipitiya, E., Margolis, H. A., Matamala, R., McCaughey, J. H., Monson, R., Munger, J. W., Oechel, W., Peng, C. H., Price, D. T., Ricciuto, D., Riley, W. J., Roulet, N., Tian, H. Q., Tonitto, C., Torn, M., Weng, E. S., and Zhou, X. L.: A model-data comparison of gross primary productivity: results from the North American Carbon Program site synthesis, J. Geophys. Res., 117, G03010, doi:10.1029/2012jg001960, 2012.

Shindell, D. T., Faluvegi, G., Unger, N., Aguilar, E., Schmidt, G. A., Koch, D. M., Bauer, S. E., and Miller, R. L.: Simulations of preindustrial, present-day, and 2100 conditions in the NASA GISS composition and climate model G-PUCCINI, Atmos. Chem. Phys., 6, 4427–4459, doi:10.5194/acp-6-4427-2006, 2006.

Shindell, D. T., Pechony, O., Voulgarakis, A., Faluvegi, G., Nazarenko, L., Lamarque, J.-F., Bowman, K., Milly, G., Kovari, B., Ruedy, R., and Schmidt, G. A.: Interactive ozone and methane chemistry in GISS-E2 historical and future climate simulations, Atmos. Chem. Phys., 13, 2653–2689, doi:10.5194/acp-13-2653-2013, 2013.

Sitch, S., Cox, P. M., Collins, W. J., and Huntingford, C.: Indirect radiative forcing of climate change through ozone effects on the land-carbon sink, Nature, 448, 791–794, doi:10.1038/Nature06059, 2007.

Spitters, C. J. T., Toussaint, H. A. J. M., and Goudriaan, J.: Separating the diffuse and direct component of global radiation and its implications for modeling canopy photosynthesis. 1. Components of incoming radiation, Agr. Forest Meteorol., 38, 217–229, doi:10.1016/0168-1923(86)90060-2, 1986.

Sun, G., McLaughlin, S. B., Porter, J. H., Uddling, J., Mulholland, P. J., Adams, M. B., and Pederson, N.: Interactive influences of ozone and climate on streamflow of forested watersheds, Glob. Change Biol., 18, 3395–3409, doi:10.1111/J.1365-2486.2012.02787.X, 2012.

Uddling, J., Teclaw, R. M., Pregitzer, K. S., and Ellsworth, D. S.: Leaf and canopy conductance in aspen and aspen-birch forests under free-air enrichment of carbon dioxide and ozone, Tree Physiol, 29, 1367–1380, doi:10.1093/Treephys/Tpp070, 2009.

Unger, N.: Global climate impact of civil aviation for standard and desulfurized jet fuel, Geophys. Res. Lett., 38, L20803, doi:10.1029/2011gl049289, 2011.

Unger, N. and Pan, J. L.: New directions: enduring ozone, Atmos. Environ., 55, 456–458, doi:10.1016/J.Atmosenv.2012.03.036, 2012.

Unger, N., Harper, K., Zheng, Y., Kiang, N. Y., Aleinov, I., Arneth, A., Schurgers, G., Amelynck, C., Goldstein, A., Guenther, A., Heinesch, B., Hewitt, C. N., Karl, T., Laffineur, Q.,

ACPD
13, 31563–31605, 2013

Langford, B., A. McKinney, K., Misztal, P., Potosnak, M., Rinne, J., Pressley, S., Schoon, N., and Serça, D.: Photosynthesis-dependent isoprene emission from leaf to planet in a global carbon-chemistry-climate model, Atmos. Chem. Phys., 13, 10243–10269, doi:10.5194/acp-13-10243-2013, 2013.

von Caemmerer, S. and Farquhar, G. D.: Some relationships between the biochemistry of photosynthesis and the gas-exchange of leaves, Planta, 153, 376–387, 1981.

Wittig, V. E., Ainsworth, E. A., and Long, S. P.: To what extent do current and projected increases in surface ozone affect photosynthesis and stomatal conductance of trees? A meta-analytic review of the last 3 decades of experiments, Plant Cell Environ., 30, 1150–1162, doi:10.1111/J.1365-3040.2007.01717.X, 2007.

Wu, S. L., Mickley, L. J., Leibensperger, E. M., Jacob, D. J., Rind, D., and Streets, D. G.: Effects of 2000–2050 global change on ozone air quality in the United States, J. Geophys. Res., 113, D06302, doi:10.1029/2007jd008917, 2008.

Xiao, J. F., Zhuang, Q. L., Law, B. E., Chen, J. Q., Baldocchi, D. D., Cook, D. R., Oren, R., Richardson, A. D., Wharton, S., Ma, S. Y., Martin, T. A., Verma, S. B., Suyker, A. E., Scott, R. L., Monson, R. K., Litvak, M., Hollinger, D. Y., Sun, G., Davis, K. J., Bolstad, P. V., Burns, S. P., Curtis, P. S., Drake, B. G., Falk, M., Fischer, M. L., Foster, D. R., Gu, L. H., Hadley, J. L., Katul, G. G., Roser, Y., McNulty, S., Meyers, T. P., Munger, J. W., Noormets, A., Oechel, W. C., Paw, K. T., Schmid, H. P., Starr, G., Torn, M. S., and Wofsy, S. C.: A continuous measure of gross primary production for the conterminous United States derived from MODIS and AmeriFlux data, Remote Sens. Environ., 114, 576–591, doi:10.1016/J.Rse.2009.10.013, 2010.

Zhang, L., Su, B. Y., Xu, H., and Li, Y. G.: Growth and photosynthetic responses of four landscape shrub species to elevated ozone, Photosynthetica, 50, 67–76, doi:10.1007/S11099-012-0004-Z, 2012.

ACPD
13, 31563–31605, 2013

Table 1. Parameters for vegetation model and O_3 damage scheme.

PFT[a]	TDA	GRAC3	GRAC4	SHR	DBF	ENF	TRF	CRO
Carboxylation	C3	C3	C4	C3	C3	C3	C3	C3/C4 [b]
V_{max} ($\mu mol\, m^{-2}\, s^{-1}$)	33	43	40	25	30	43	54	40
m	9	11	9	9	9	9	9	9
b ($mmol\, m^{-2}\, s^{-1}$)	2	8	2	2	2	2	2	2
O_3T ($nmol\, m^{-2}\, s^{-1}$)	1.6	5	5	1.6	1.6	1.6	1.6	5
a (high) ($mmol^{-1}\, m^{-2}$)	0.1	1.4	0.735	0.1	0.15	0.075	0.15	1.4
a (low) ($mmol^{-1}\, m^{-2}$)	0.03	0.25	0.13	0.03	0.04	0.02	0.04	0.25

[a] Plant function types (PFTs) are tundra (TDA), C3 grassland (GRAC3), C4 savanna/grassland (GRAC4), shrubland (SHR), deciduous broadleaf forest (DBF), evergreen needleleaf forest (ENF), tropical rainforest (TRF), and cropland (CRO).

[b] For site-level simulations, we consider CRO as C4 plant. For regional simulation, we consider CRO as C3 plant. See explanation in Sect. 2.2.2.

ACPD
13, 31563–31605, 2013

Table 2. Match of model PFTs with that from NACP sites and the ISLSCP dataset.

PFTs in the model	PFTs at NACP sites	PFTs from ISLSCP
Tundra	N/A	N/A
C3 grassland	Grasslands	Grasslands
C4 grassland	N/A	Savannas
Shrubland	Closed Shrubland	Closed Shrubland
	Woody Savannas	Open Shrubland
	Permanent Wetlands	Woody Savannas
		Permanent Wetlands
Deciduous Broadleaf Forest	Deciduous Broadleaf Forest	Deciduous Needleleaf Forest
		Deciduous Broadleaf Forest
Evergreen Needleleaf Forest	Evergreen Needleleaf Forest	Evergreen Needleleaf Forest
	Mixed Forests	Mixed Forests
Tropical Rainforest	N/A	Evergreen Broadleaf Forest
Cropland	Croplands (C4)	Croplands (C3)
		Cropland/Natural vegetation mosaic (C3)

ACPD
13, 31563–31605, 2013

Table 3. Description of the site-level simulations.

ID	Simulations	Meteorology		Phenology (LAI)		Incl. O_3 [a]
		Site	MERRA	MODIS	MERRA	
1	MERRA_MODIS		Yes	Yes		
2	SITEM_MODIS	Yes	Yes	Yes		
3	MERRA_VEG		Yes		Yes	
4	SITEM_VEG	Yes	Yes		Yes	
5	SITEM_VEG_LO3	Yes	Yes		Yes	Low [b]
6	SIETM_VEG_HO3	Yes	Yes		Yes	High [b]

[a] Ambient [O_3] is applied at each site.

[b] Low and high indicate the sensitivity of GPP to [O_3].

ACPD
13, 31563–31605, 2013

Table A1. Descriptions of NACP sites [a].

Site	PFT [b]	Description	Longitude	Latitude	Period
CA-Ca1	ENF	Campbell River	125.3° W	49.9° N	1998–2006
CA-Ca2	ENF	Campbell River	125.3° W	49.9° N	2001–2006
CA-Ca3	ENF	Campbell River	124.9° W	49.5° N	2002–2006
CA-Gro	MF	Groundhog River	82.2° W	48.2° N	2004–2006
CA-Let	GRA	Lethbridge Grassland	112.9° W	49.7° N	2001–2007
CA-Mer	WET	Eastern Peatland	75.5° W	45.4° N	1999–2006
CA-NS1	ENF	UCI Chronosequence	124.9° W	49.5° N	2001–2005
CA-Oas	DBF	BERMS	106.2° W	53.6° N	1997–2006
CA-Obs	ENF	BERMS	105.1° W	54.0° N	2000–2006
CA-Ojp	ENF	BERMS	104.7° W	53.9° N	2000–2006
CA-Qfo	ENF	Quebec	74.3° W	49.7° N	2004–2006
CA-SJ1	ENF	BERMS	104.7° W	53.9° N	2002–2005
CA-SJ2	ENF	BERMS	104.6° W	53.9° N	2004–2006
CA-SJ3	ENF	BERMS	104.6° W	53.9° N	2005–2006
CA-TP4	ENF	Turkey Point	80.4° W	42.7° N	2003–2007
CA-WP1	WET	Western Peatland	112.5° W	55.0° N	2004–2007
US-ARM	CRO	Southern Great Plains	97.5° W	36.6° N	2003–2007
US-Dk3	ENF	Duke Forest	79.1° W	36.0° N	1998–2005
US-Ha1	DBF	Harvard Forest	72.2° W	42.5° N	1992–2006
US-Ho1	ENF	Howland Forest	68.7° W	45.2° N	1996–2004
US-IB1	CRO	Fermi Lab	88.2° W	41.9° N	2006
US-IB2	GRA	Fermi	88.2° W	41.8° N	2005–2006
US-Los	WET	Lost Creek	90.0° W	46.1° N	2001–2006
US-MMS	DBF	Morgan Monroe State Forest	86.4° W	39.3° N	1999–2006
US-MOz	DBF	Missouri Ozark	92.2° W	38.7° N	2005–2007
US-Me2	ENF	Metolius	121.6° W	44.5° N	2002–2007
US-Me3	ENF	Metolius	121.6° W	44.3° N	2004–2005
US-Me5	ENF	Metolius	121.6° W	44.4° N	2000–2002
US-NR1	ENF	Niwot Ridge	105.5° W	40.0° N	1999–2007
US-Ne1	CRO	Mead	96.5° W	41.2° N	2002–2005
US-Ne2	CRO	Mead	96.5° W	41.2° N	2003–2005
US-Ne3	CRO	Mead	96.4° W	41.2° N	2002–2005
US-Pfa	MF	Park Falls	90.3° W	45.9° N	1997–2004
US-SO2	CSH	Sky Oaks	116.6° W	33.4° N	1999–2006
US-Shd	GRA	Shidler	96.7° W	36.9° N	1998–1999
US-Syv	MF	Sylvania Wilderness Area	89.3° W	46.2° N	2002–2006
US-Ton	WSA	Tonzi Ranch	121.0° W	38.4° N	2002–2007
US-UMB	DBF	UMBS	84.7° W	45.6° N	1999–2006
US-Var	GRA	Varia Ranch	121.0° W	38.4° N	2001–2007
US-WCr	DBF	Willow Creek	90.1° W	45.8° N	1999–2006

[a] Site information is adopted from Schaefer et al. (2012), except that the operational time span listed here is only for the period when measurements of GPP are available.
[b] PFT names are: evergreen needleleaf forest (ENF), deciduous broadleaf forest (DBF), grasslands (GRA), croplands (CRO), closed shrublands (CSH), mixed forests (MF), permanent wetlands (WET), and woody savannas (WSA).

ACPD
13, 31563–31605, 2013

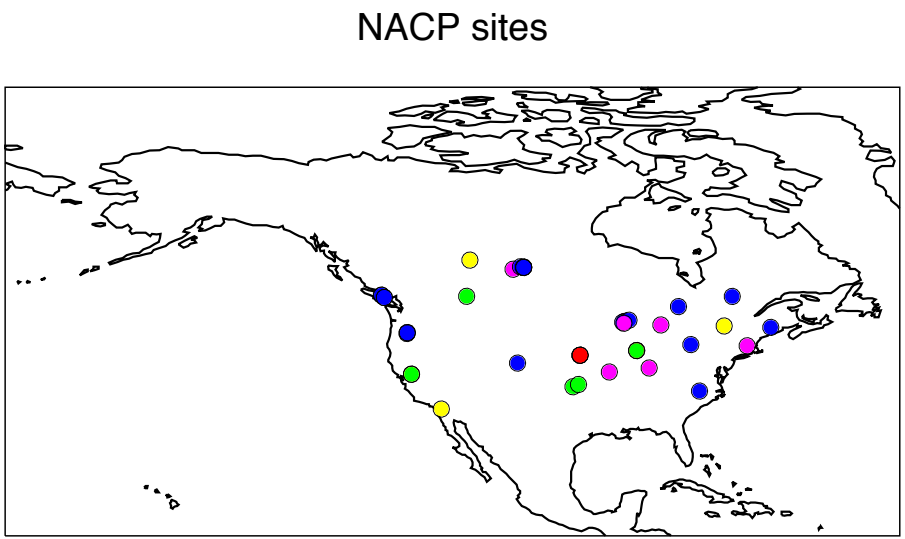

Fig. 1. Distribution of 40 North American Carbon Program (NACP) sites. The color indicates different land types as evergreen needleleaf forest (ENF, blue), deciduous broadleaf forest (DBF, magenta), grasslands (GRA, green), croplands (CRO, red), shrublands (SHR, yellow). "Mixed Forests" are classified as ENF, "Permanent Wetlands" and "Woody Savannas" as SHR (Table 2). The local vegetation type at each site is described in appendix Table A.

ACPD
13, 31563–31605, 2013

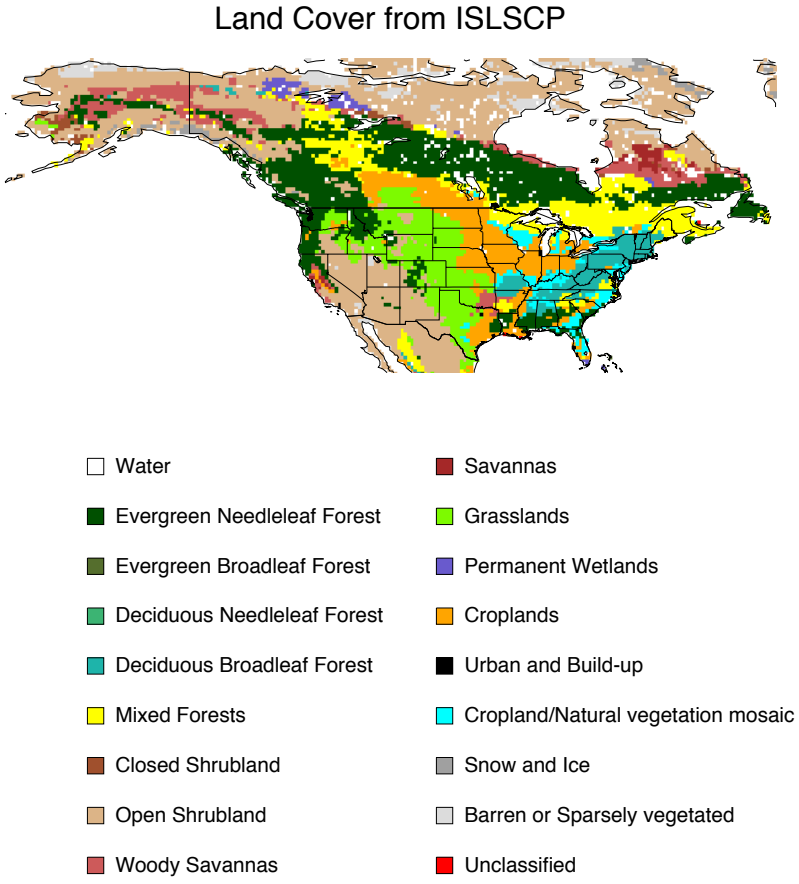

Fig. 2. Land cover types in North America developed by the International Satellite Land-Surface Climatology Project (ISLSCP).

ACPD
13, 31563–31605, 2013

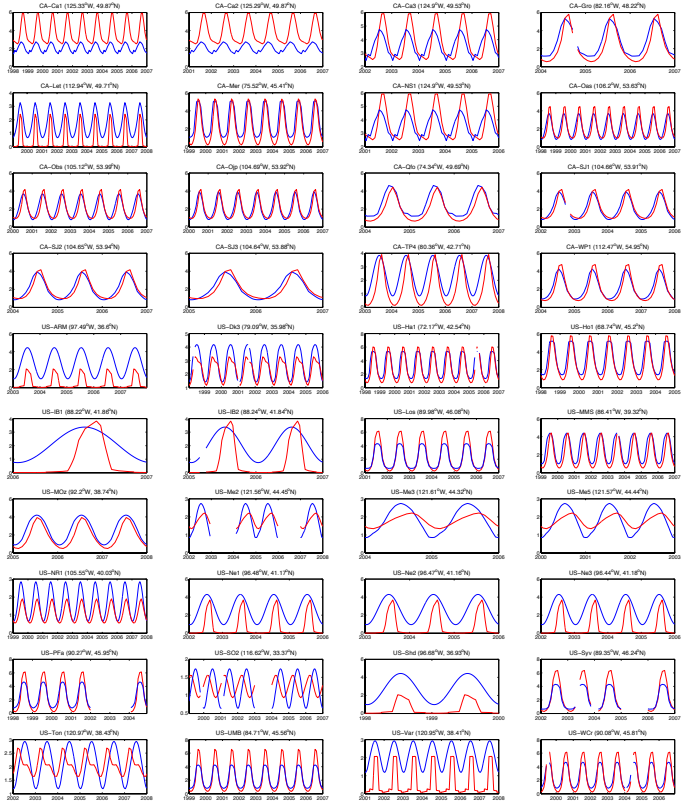

Fig. 3. Comparison of daily average leaf area index (LAI, $m^2\,m^{-2}$) from the Modern Era-Retrospective Analysis (MERRA) reanalysis (red) and the Moderate Resolution Imaging Spectroradiometer (MODIS) (blue) at each NACP site. The daily average LAI is shown only when gross primary productivity (GPP) measurements are available at the site.

ACPD
13, 31563–31605, 2013

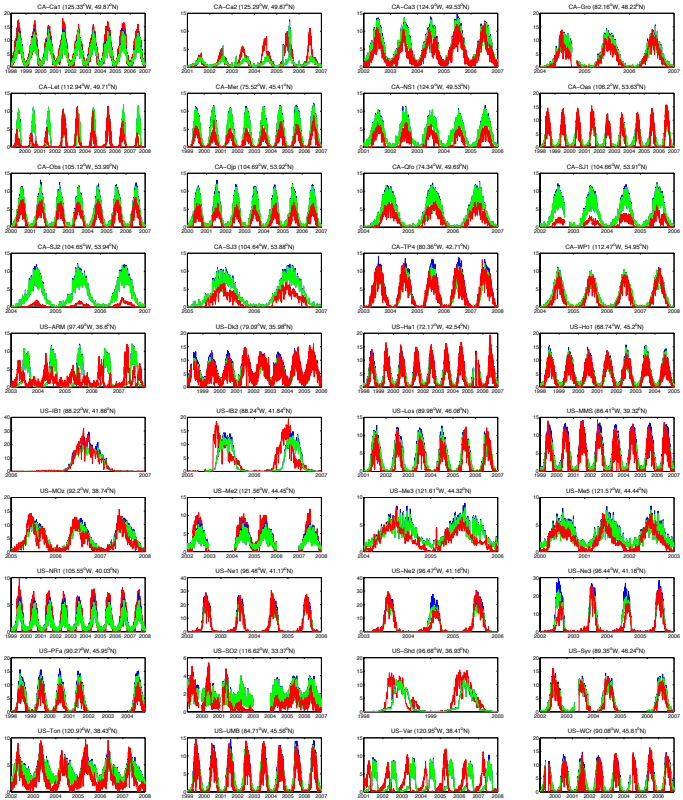

Fig. 4. Comparison of daily GPP ($g C m^{-2} day^{-1}$) from observations (red) and simulations with (green) and without (blue) O_3 damage effects at each site. The simulation, SITEM_VEG, is driven with meteorological forcings from MERRA and site measurements. The LAI is from MERRA. The O_3 damage effect is estimated with high O_3 sensitivity. The time span is different for each site.

ACPD
13, 31563–31605, 2013

Ozone vegetation damage effects on gross primary productivity in the US

X. Yue and N. Unger

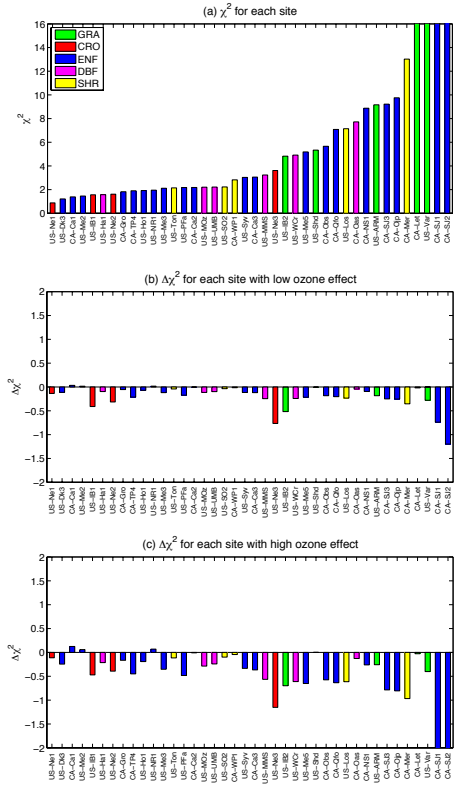

Fig. 5. The calculated **(a)** χ^2 of GPP and changes in χ^2 after the inclusion of O_3 damage impact with **(b)** low and **(c)** high O_3 sensitivity at each site. The sites are sorted according to the values of χ^2 in **(a)**. The land cover definitions are: GRA, Grasslands; CRO, Croplands; ENF, Evergreen Needleleaf Forest; DBF, Deciduous Broadleaf Forest; SHR, Shrubland.

ACPD
13, 31563–31605, 2013

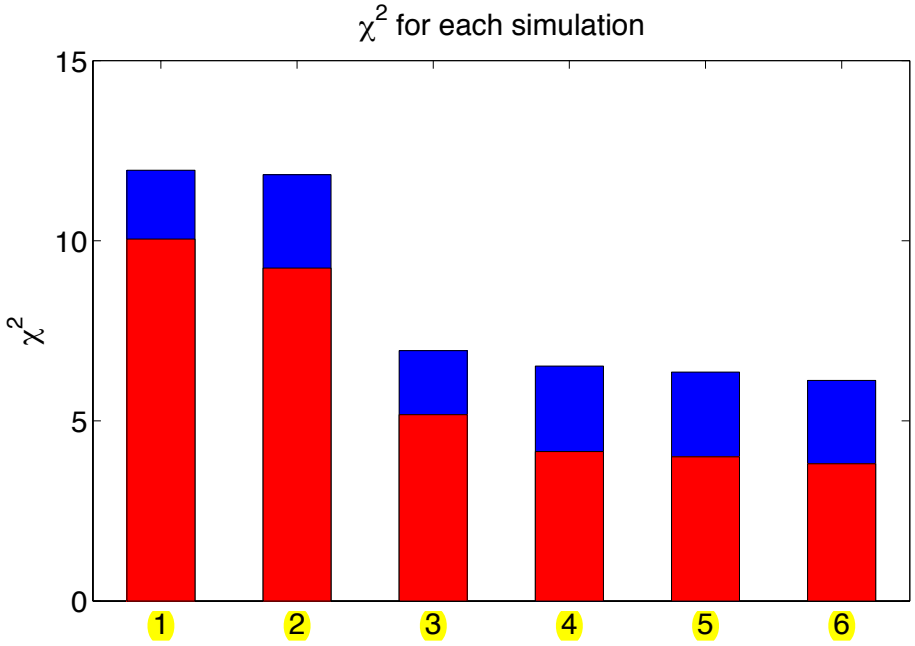

Fig. 6. The calculated average χ^2 of GPP over NACP sites for 6 different simulations as listed in Table 3. The blue bars are results for all 40 NACP sites. The red bars are results excluding sites CA-Let, US-Var, CA-SJ1, and CA-SJ2, where the simulated site-level χ^2 is larger than 16 as shown in Fig. 5a.

ACPD
13, 31563–31605, 2013

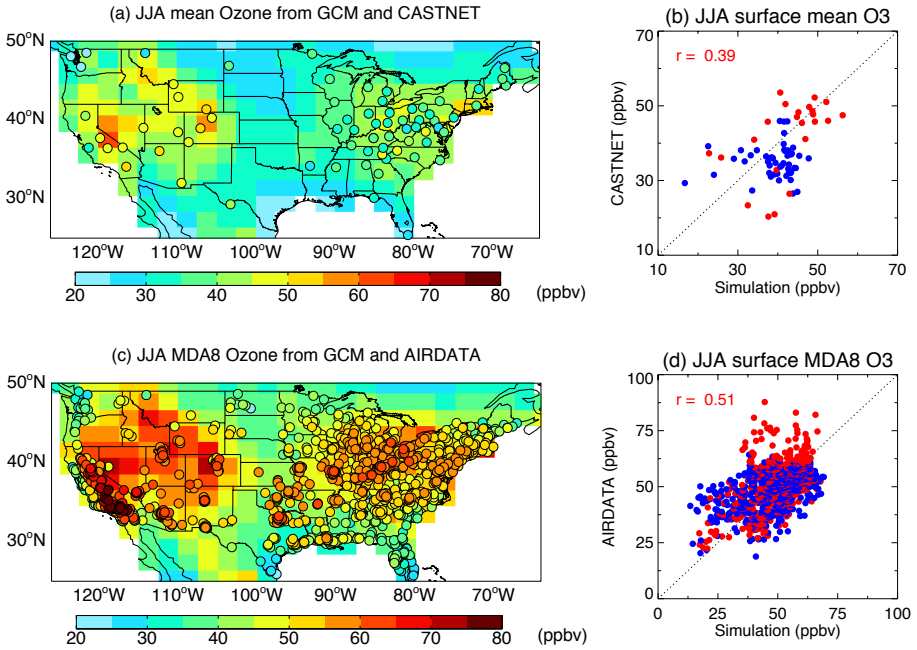

Fig. 7. Validation of simulated summertime surface **(a** and **b)** diurnal mean and **(c** and **d)** daily maximum 8 h average O_3 with in situ measurements from **(a** and **b)** the EPA Clean Air Status and Trends Network (CASTNET) and **(c** and **d)** the AIRDATA. For **(b)** and **(d)**, the blue points indicate sites East of 95° W and the red ones for West of 95° W. The correlation coefficients between simulations and observations are shown in **(b)** and **(d)**.

ACPD
13, 31563–31605, 2013

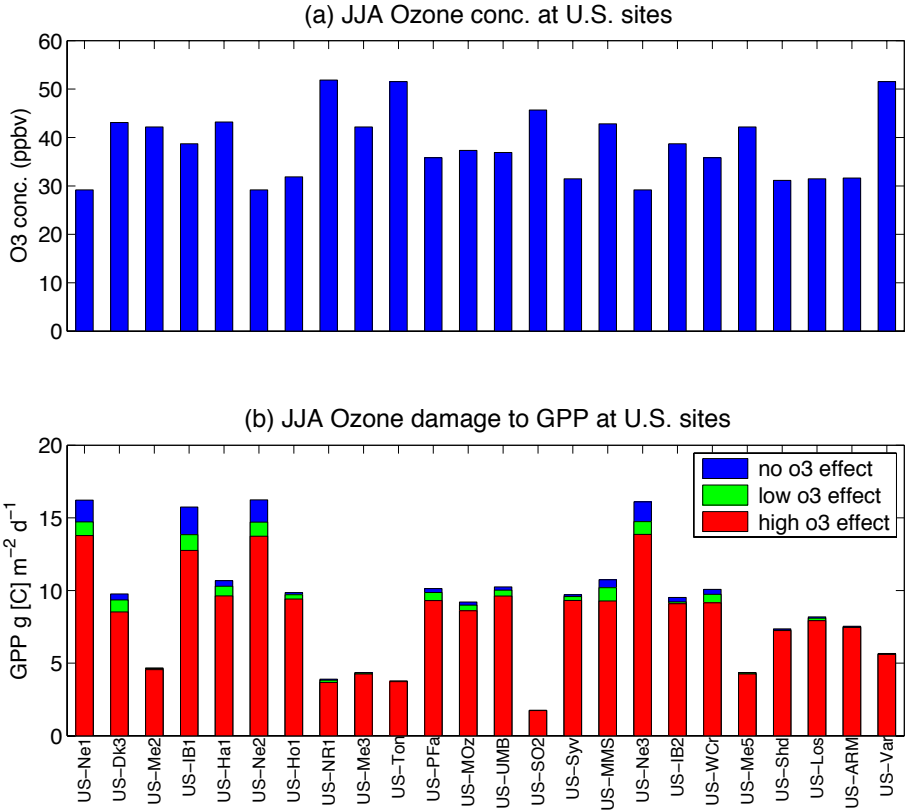

Fig. 8. Simulated **(a)** surface [O_3] and **(b)** damages to GPP at different O_3 sensitivity for 24 US sites. The sites are sorted according to the values of χ^2 calculated in Fig. 5a.

ACPD
13, 31563–31605, 2013

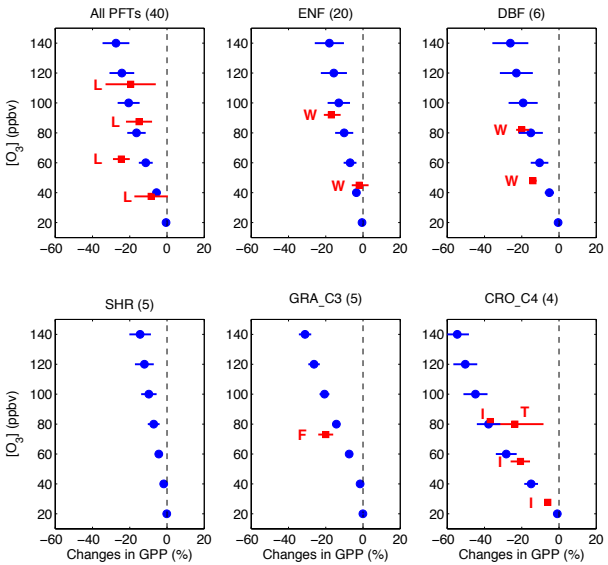

Fig. 9. Changes in GPP for all and individual PFTs in the presence of different levels of [O_3] as simulated by the vegetation model. Simulations are performed at 40 NACP sites with a fixed [O_3] for either low or high O_3 sensitivity. The blue lines show the damages ranging from low to high O_3 sensitivity, with the blue points indicating the average reductions. The simulation results are averaged for all the sites or for the sites with the same PFT. The number of sites used for average is shown in the title bracket of each subplot. The red squares with lines show the results (mean plus uncertainty) based on measurements reported by multiple literatures. These measurements are collected by Lombardozzi et al. (2013) for all PFTs, Wittig et al. (2007) for ENF (evergreen needleleaf forest) and DBF (deciduous broadleaf forest), Feng et al. (2008) for wheat, Ishii et al. (2004) for rice, and Taylor et al. (2002) for a C4 grass. The author initials are indicated for the corresponding studies.

ACPD
13, 31563–31605, 2013

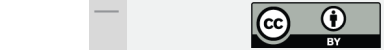

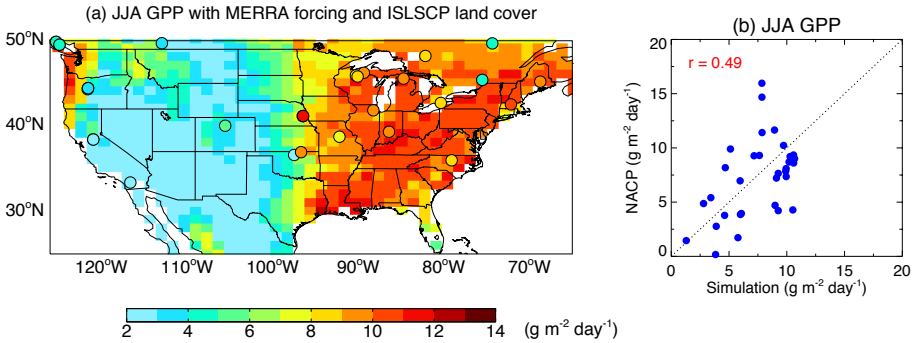

Fig. 10. Validation of simulated summertime GPP over the US with in situ measurements from NACP. The simulations are performed with land cover from ISLSCP and meteorological forcings from Modern Era-Retrospective Analysis (MERRA) reanalyses. Each point in **(b)** indicates a NACP site below 50° N.

ACPD
13, 31563–31605, 2013

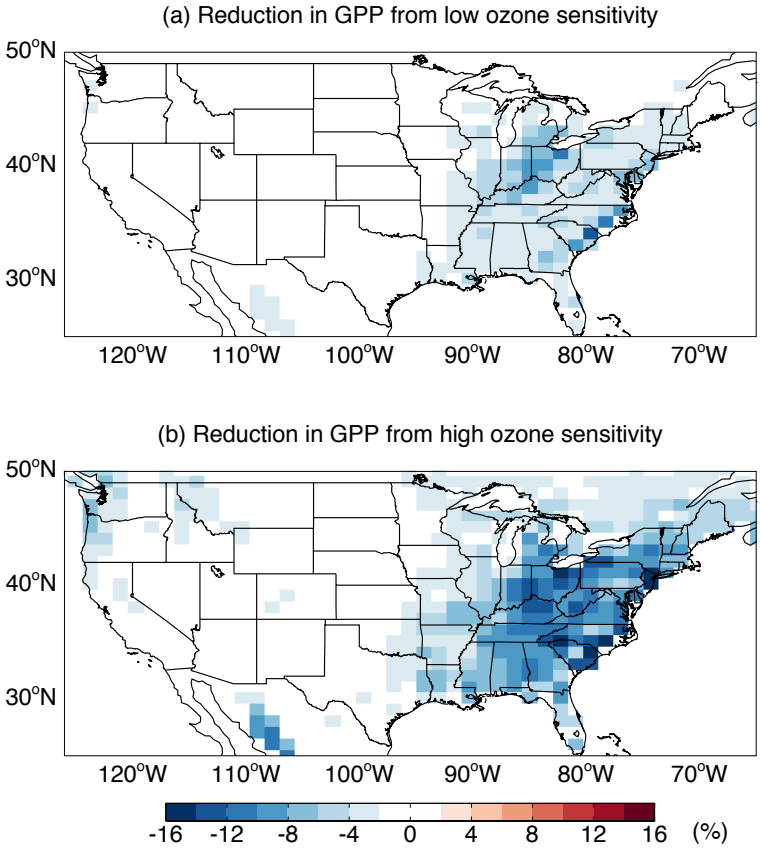

Fig. 11. Simulated reduction fraction in summer GPP in the US due to **(a)** low and **(b)** high O_3 sensitivity.

ACPD
13, 31563–31605, 2013

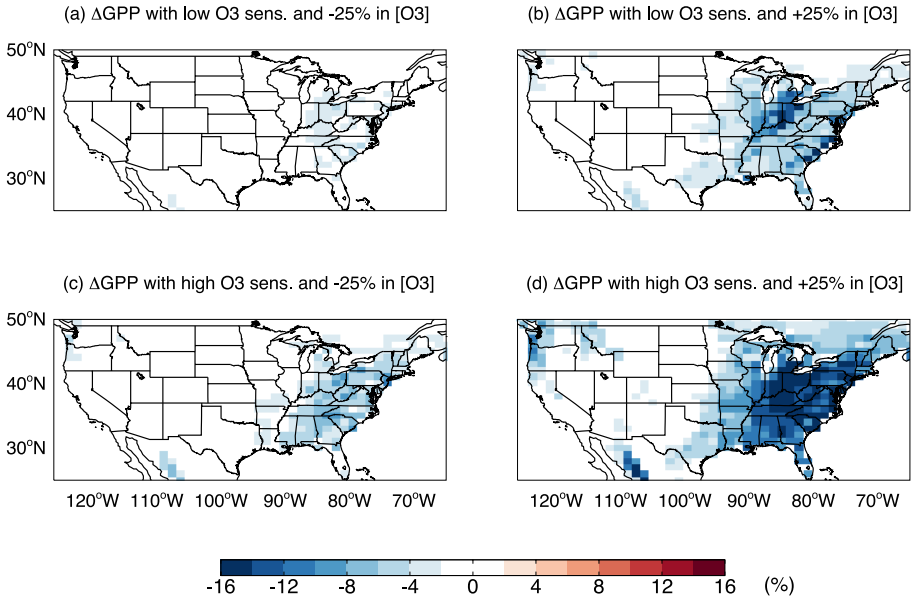

Fig. 12. Simulated changes in summer GPP due to **(a** and **c)** 25 % reduction or **(b** and **d)** 25 % increase in [O_3] for **(a** and **b)** low or **(c** and **d)** high O_3 sensitivity.

ACPD
13, 31563–31605, 2013